nature chemistry

Perspective

https://doi.org/10.1038/s41557-022-01056-2

Challenges to developing materials for the transport and storage of hydrogen

Received: 14 October 2020

Accepted: 2 September 2022

Published online: 27 October 2022

Check for updates

Mark D. Allendorf[1] ✉, Vitalie Stavila[1], Jonathan L. Snider[1], Matthew Witman[1], Mark E. Bowden[2] ✉, Kriston Brooks[2], Ba L. Tran[2] and Tom Autrey[2]

Hydrogen has the highest gravimetric energy density of any energy carrier and produces water as the only oxidation product, making it extremely attractive for both transportation and stationary power applications. However, its low volumetric energy density causes considerable difficulties, inspiring intense efforts to develop chemical-based storage using metal hydrides, liquid organic hydrogen carriers and sorbents. The controlled uptake and release of hydrogen by these materials can be described as a series of challenges: optimal properties fall within a narrow range, can only be found in few materials and often involve important trade-offs. In addition, a greater understanding of the complex kinetics, mass transport and microstructural phenomena associated with hydrogen uptake and release is needed. The goal of this Perspective is to delineate potential use cases, define key challenges and show that solutions will involve a nexus of several subdisciplines of chemistry, including catalysis, data science, nanoscience, interfacial phenomena and dynamic or phase-change materials.

Hydrogen has the highest gravimetric energy density of any energy carrier — with a lower heating value (LHV) of 120 MJ kg^{-1} at 298 K versus 44 MJ kg^{-1} for gasoline — and produces only water when used to power a fuel cell. As an energy vector, it is also scalable, creating opportunities when alternatives are too expensive, too heavy or have insufficient capacity. Realizing this powerful approach to decarbonizing the energy economy will require its transport and storage in the form of chemical bonds[1]. Hydrogen-rich compounds can serve as a storage medium for both mobile and stationary applications, but can also address the intermittency of renewable power sources where large-scale energy storage for extended time periods is needed. However, the requirements of stationary use cases are very different from those of transportation (Table 1)[2–4].

Recent analysis indicates that the slow pace of infrastructure development for hydrogen transport and storage is affecting its economics and consumer appeal[2]. A major barrier is the low hydrogen volumetric energy density, which is 27 $gH_2\ l^{-1}$ at the 700-bar pressure used in commercially available fuel cell electric vehicles. This falls short of the 50 $gH_2\ l^{-1}$ ultimate target set by the US Department of Energy (DOE) for light-duty vehicles[5]. Although cryo-compressed hydrogen has a higher value (44 $gH_2\ l^{-1}$), it is uneconomical for some applications[6]. Consequently, material-based storage is essential if both mobile and stationary use cases are to be realized.

Thermodynamically, hydrogen storage is a classic 'Goldilocks challenge', in which the optimal Gibbs free energy change ($\Delta G°$) for practical applications falls within a narrow range and achieving it may necessitate trade-offs with other properties. Hydrogen release and uptake at moderate temperatures and pressures require a low absolute value of $\Delta G°$, but enthalpy considerations have dominated material design. Dehydrogenation enthalpies ($\Delta H°$) of 15–25 kJ $molH_2^{-1}$ maximize the sorbent deliverable capacity at ambient temperature[7], whereas modelling suggests that $\Delta H° \cong 27$ kJ $molH_2^{-1}$ is optimal to allow desorption from metal hydrides using only residual heat from a fuel cell[8]. Consequently, optimal chemistries for storage under ambient conditions fall into an energy no-man's land: hydrogen-binding energies are either too strong (complex metal hydrides, small molecules such as NH_3, and liquid hydrocarbons) or too weak (sorbents). Complicating the issue is the wide range of dehydrogenation entropies,

[1]Sandia National Laboratories, Livermore, CA, USA. [2]Pacific Northwest National Laboratory, Richland, WA, USA. ✉e-mail: mdallen@sandia.gov; mark.bowden@pnnl.gov

https://doi.org/10.1038/s41557-022-01056-2

Table 1 | Examples of use cases for hydrogen carriers, illustrating a range of power, energy, hydrogen usage and storage requirements

Use case[a]	Relative size	Power (MW)[b]	Energy (MWh)[c]	H_2 usage (kg d^{-1})[d]	Use duration (d)[e]	H_2 rate (kg h^{-1})[f]	Basis reference
Mobile applications							
Light-duty vehicle	Small	0.08	0.078	0.76	365	0.56	Ref. [5]
Long-haul truck	Medium	0.24	0.8	60	365	5.4	Ref. [146]
Refuel medium-duty fleet	Large	0.83	NA	1,000	365	41.7	Ref. [147]
High-speed ferry	Very large	4.9	17	2,000	365	210	Ref. [148]
Regional fuel depot	Extreme	41.7	NA	50,000	365	2,083	Ref. [149]
Stationary applications							
Telecom backup	Small	0.003	0.2	3.5	3	0.14	Ref. [150]
Seasonal microgrid storage	Medium	0.027	85	39	130	1.6	Ref. [151]
International shipping	Large	0.48	N/A	575	365	24	Ref. [152]
Hospital backup	Large	0.59	99	709	7	29	Ref. [153]
Data centre backup	Very large	20	1,440	30,000	3	1,250	Ref. [154]
Grid-scale long-duration storage	Extreme	100	1,000	120,000	0.42	5,000	Ref. [155]
Steel mill DRI	Extreme	250	NA	300,000	365	12,500	Ref. [45]

This table shows how the number of applications under consideration has expanded dramatically from the early focus on transportation (especially light-duty vehicles) to include stationary (grid-scale storage), mobile energy storage (international shipping) and chemical reductant (for example, decarbonizing heavy industries such as steel production). [a]For details on the basis for the values in the table, see the Supplementary Information (Section 1). [b]Maximum instantaneous power required, or that would be produced from the fuel cell. [c]Maximum energy or hydrogen storage required between refuelling events. [d]Average H_2 usage per day based on the yearly average. [e]Period of expected continuous operation, up to 1 year. [f]Average H_2 usage during operation, or equivalently, required dehydrogenation rate of the hydrogen storage material or carrier. DRI, direct reduced iron; NA, not applicable.

$\Delta S°$[9,10], which are often approximated as $8R$ (that is, 66.5 J mol^{-1} K^{-1}, where R is the gas constant) for sorbents[9] and 130.7 J mol^{-1} K^{-1} (gaseous H_2) for metal hydrides, probably because it is difficult to predict and structure–property relationships are lacking. As will be evident below, however, thermodynamics is only one of several hydrogen storage challenges.

In this Perspective, we assess the primary challenges within the major storage material classes: liquid organic hydrogen carriers (LOHC)[11–14], metal hydrides (both bulk[15] and nanoscale[16]); and metal–organic framework adsorbents (MOFs)[7]. The chemical challenges are defined in part by engineering considerations, which are in turn set by application-specific energy and power requirements (Table 1). For example, the development of robust catalysts to meet H_2 release rates for specific use cases must take into account the practical limitations of industrial reactors. It is also clear that surmounting the challenges facing practical hydrogen storage will engage subdisciplines on the forefront of chemistry: single-site[17], electrochemical[11] and homogeneous[18,19] catalysis; nanoscale and chemical confinement effects[16,20]; reactions at buried interfaces[21]; quantum chemistry of weak interactions[7,22]; sorption at strong binding sites[23,24]; dynamic or phase-change sorbents[25–27]; and machine learning and data science[10,28].

Hydrogen use cases

Although hydrogen has long been recognized as a versatile energy carrier, much of the research has focused on transportation, driven by detailed US DOE technical targets (Fig. 1)[5]. For the many other use cases (Table 1), such targets do not exist. For example, compensating for intermittent renewable energy generation is an often-cited motivation for developing reversible hydrogen storage materials, but research has typically focused on cross-cutting needs rather than specific use cases (for example, robust catalysts to enable reversible hydrogen release from LOHCs). The range of delivery rates (Table 1), reaction conditions (Supplementary Table 1) and purity requirements indicate there is no one-size-fits-all material. Instead, material selection is typically governed by trade-offs among thermodynamics, kinetics and capacity. Thermodynamics typically limits the capacity of sorbents and main-group hydrides such as MgH_2 and LiH (Fig. 2), which require undesirable reaction conditions to store, release or regenerate the material. In contrast, kinetic barriers are often rate limiting for LOHCs and complex metal hydrides, requiring new strategies to enable H_2 release/uptake under practical conditions. Moreover, high selectivity for X–H bond activation (where X = C, N, B, O or metal) is essential to avoid kinetic sinks and control hydrogen purity. Consequently, material development must start with the use case requirements rather than simply the theoretical maximum hydrogen capacity.

LOHCs

LOHCs—small organic molecules that are liquid under ambient conditions and can be reversibly hydrogenated and dehydrogenated, such as methanol, formic acid or cycloalkanes—are attractive because they are readily adapted to existing infrastructure. Recent reviews discuss their benefits and efforts to develop effective catalysts for their hydrogenation and dehydrogenation[14,29–32]. Here, we consider the specific demands (power, energy, hydrogen capacity and average dehydrogenation rate) for various use cases (Table 1) and propose optimal LOHC physiochemical properties (Supplementary Table 2). To define these, we considered the efficiency of H_2 release and regeneration, transport, storage, handling, separations and purification, as well as reaction rates and mass transport limits for catalysed H_2 release and regeneration. Thus, not only basic thermodynamics and kinetics must be considered, but also properties such as the melting point, vapour pressure, viscosity, reversibility and conversion.

In general, LOHCs having only liquid-phase dehydrogenated products facilitate the use of existing infrastructure and avoid the transport and capture of gas-phase species such as CO_2 and CO. However, this creates a conflict, as the desirable reaction thermodynamics cause other physical properties to be suboptimal. A low melting point (<−20 °C) and vapour pressure (<0.01 atm at 50 °C), for example, facilitate H_2 separation (>99% pure H_2 is achievable using a simple air condenser), while low viscosity reduces the pumping requirements, but these properties are frequently in opposition. Comparing methylcyclohexane with other LOHCs provides a useful illustration. Although the H_2 content of methylcyclohexane (47 kgH_2 m^{-3}) is less than that of decalin or cyclohexane, it is nevertheless >50% higher than 250-bar compressed

https://doi.org/10.1038/s41557-022-01056-2

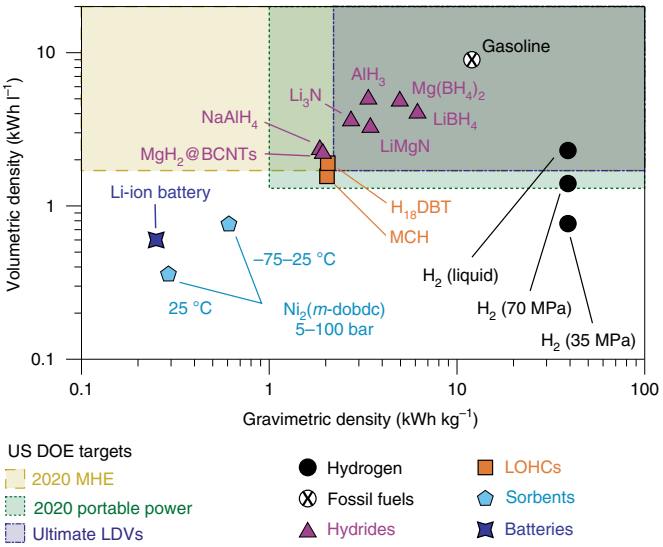

Fig. 1 | Comparison of the volumetric and gravimetric energy densities of hydrogen storage materials with US DOE technical targets. The volumetric and gravimetric energy densities of many hydrogen storage materials exceed those of batteries, but unfavourable hydrogen-binding energies continue to be a challenge for practical implementation. Energy needs vary dramatically in both power and time, as shown by these material classes adapted from the International Energy Agency's *Technology Roadmap—Hydrogen and Fuel Cells*[126]. Hydrogen-based strategies for high-density energy storage[127–129] include compressed gas, cryogenic liquid (black circles)[130], hydrogen chemically bound as a hydride[63,131–136] (purple triangles) or as an LOHC[32] (orange squares) or hydrogen physisorbed within a porous adsorbent[24] (light-blue pentagons). The densities of promising materials are shown against the system-based density targets set by the US DOE for light-duty vehicles (LDVs; grey shading), materials-handling equipment (MHE; yellow shading) and portable power applications (green shading)[137]. The data are shown as materials-based densities since mass and volume penalties vary with system design and end-use application. For example, in a slurry-phase vehicle system, the hydrogen storage material accounts for ≈40% of the system mass[138]. Alternatively, in cryo-adsorbent systems, the material accounts for ≈20% of the system mass and 50% of the system volume[139]. BCNT, bamboo-shaped carbon nanotubes.

H_2 (≈17 kgH_2 m^{-3}). It is also a non-viscous liquid at −20 °C, whereas both cyclohexane and benzene are solid at 5 °C. These attributes are offset by the large enthalpy for H_2 release ($\Delta H°$ ≈68 kJ mol H_2^{-1}) and high vapour pressure at 50 °C, reducing H_2 release efficiency and complicating purification.

Computational studies show that installing heteroatoms in the arene ring substantially reduces $\Delta H°$[33], making perhydro-*N*-ethylcarbazole (H12-NEC; 54 kgH_2 m^{-3}) of great interest. This molecule has both lower $\Delta H°$ (≈50 kJ molH_2^{-1}) and lower vapour pressure at 50 °C, plus fast kinetics for the release and uptake of hydrogen. Unfortunately, the hydrogen-rich form is a solid at room temperature, necessitating strategies to maintain the liquid phase by using additives or avoiding complete conversion[34]. Another computational study considered LOHCs with heteroatoms, suggesting that ethanolamine is not as stable as was previously assumed; thus, dehydrogenative coupling of 2-aminoethanol to form 2,5-piperazinedione has a lower reaction enthalpy than H12-NEC dehydrogenation[35]. In this case, the hydrogen-lean product is a solid with a melting point of >300 °C. Alcohols such as ethanol[36], butanediol[37], ethylene glycol[12], 2-aminoethanol[38] and aqueous formate[11,39,40] could be an alternative, balancing capacity against favourable liquid-phase (de)hydrogenation thermodynamics. However, the dehydrogenation rates are much lower than for cyclic alkanes. Consequently, a critical challenge is to develop catalysts and operating conditions for reactions that do not involve phase changes from liquids to solids.

The wide range of dehydrogenation rates in Table 1 underscores the importance of designing catalysts for specific applications. A single catalyst for both dehydrogenation and rehydrogenation is advantageous, particularly for stationary applications. Maximizing the turnover frequency (TOF) has often motivated catalyst development; however, analysis by Weisz[41,42] showed that this is not always necessary. Nevertheless, trade-offs among reaction kinetics, mass transfer, reactor size limitations and product purity are required. The maximum rate of most industrial chemical processes is 1–10 mol s^{-1} m^{-3} of reactor volume (≈7–70 kgH_2 h^{-1} m^{-3}), allowing the reactor size and TOF to be estimated for various use cases. To illustrate, a bed of 2% Pd/C catalyst pellets with a density of 360 kg m^{-3} contains 67.7 mol m^{-3} Pd. A catalyst dispersion of 40% leads to a modest TOF of 0.37 s^{-1} to reach the upper limit of the Weisz window while minimizing the reactor size. To meet use case power requirements, this TOF must be the average needed to fully dehydrogenate—not simply the maximum (usually initial) rate. For example, a high TOF of 17.5 s^{-1} was reported for H12-NEC dehydrogenation, but only 20% of the available hydrogen was released[43], necessitating a fivefold larger storage tank than was theoretically required. Moreover, because 80% of the LOHC would be unreacted, transportation costs to rehydrogenation facilities would increase.

These constraints notwithstanding, the lack of economical, selective and robust (de)hydrogenation catalysts is a key barrier for LOHCs, regardless of application. Although precious-metal catalysts can dehydrogenate cycloalkanes such as methylcyclohexane[44] at the maximum Weisz rate with acceptable selectivity and stability, they are probably not economically viable for medium-to-large-scale use cases (Table 1)[45]. Consequently, strategies to replace precious metals have focused primarily on supported metals[14] such as Ni[46] and bimetallics such as NiZn[47]. Alternatives are emerging, however. Homogeneous Ru- and Ir-based catalysts are promising for the dehydrogenation of *N*-heteroaromatics[48], alcohols[49] and ethylene glycol[12]. We uncovered an unexpected avenue incorporating elements of both heterogeneous

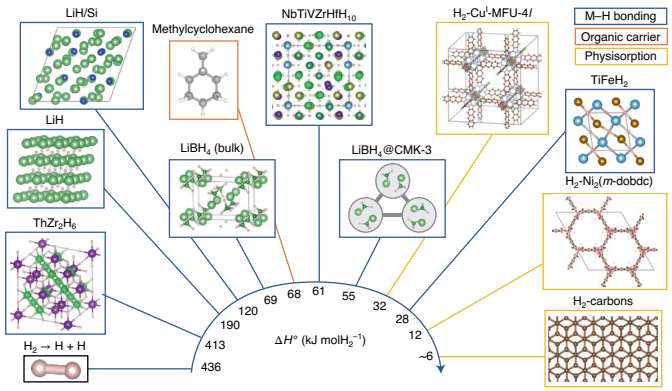

Fig. 2 | The $\Delta H°$ values of hydrogen storage materials span an enormous range. For the most stable metal hydrides (for example, $ThZr_2H_6$; Th, purple; Zr, green; H, light pink)[140] $\Delta H°$ is similar to the H–H bond energy. Doping (for example, LiH/Si; Li, green; Si, blue; H omitted)[141] and nanoconfinement (for example, $LiBH_4$@CMK-3; Li, light green; B, dark green; H, light pink; C, grey)[142] can reduce $\Delta H°$ relative to unalloyed or bulk materials, respectively. LOHCs (for example, methylcyclohexane; C, grey; H, white) typically have similar $\Delta H°$[143]. High-entropy alloys (for example, $NbTiVZrHfH_{10}$; Nb, purple; Ti, blue; V, yellow; Zr, light green; Hf, dark green; H, light pink) are a nascent class of hydrogen storage materials; their vast combinatorial composition space suggests the potential for substantial thermodynamics tunability[144]. Some interstitial metal hydrides (for example, $TiFeH_2$; Ti, blue; Fe, orange; H, light pink) have such low $\Delta H°$ that dehydrogenation occurs near ambient temperature[145]. Physisorption of hydrogen on typical porous materials, such as MOFs or ordered mesoporous carbons, is too weak for practical capacity above cryogenic temperatures. Two MOFs, Ni_2(*m*-dobdc)[24] and Cu^I-MFU-4*l*[92], are exceptions, having appreciable room temperature uptake due to a high isosteric heat of adsorption afforded by open metal sites (C, brown; O, red; Ni, grey; Cl, green; N, blue; H, white).

https://doi.org/10.1038/s41557-022-01056-2

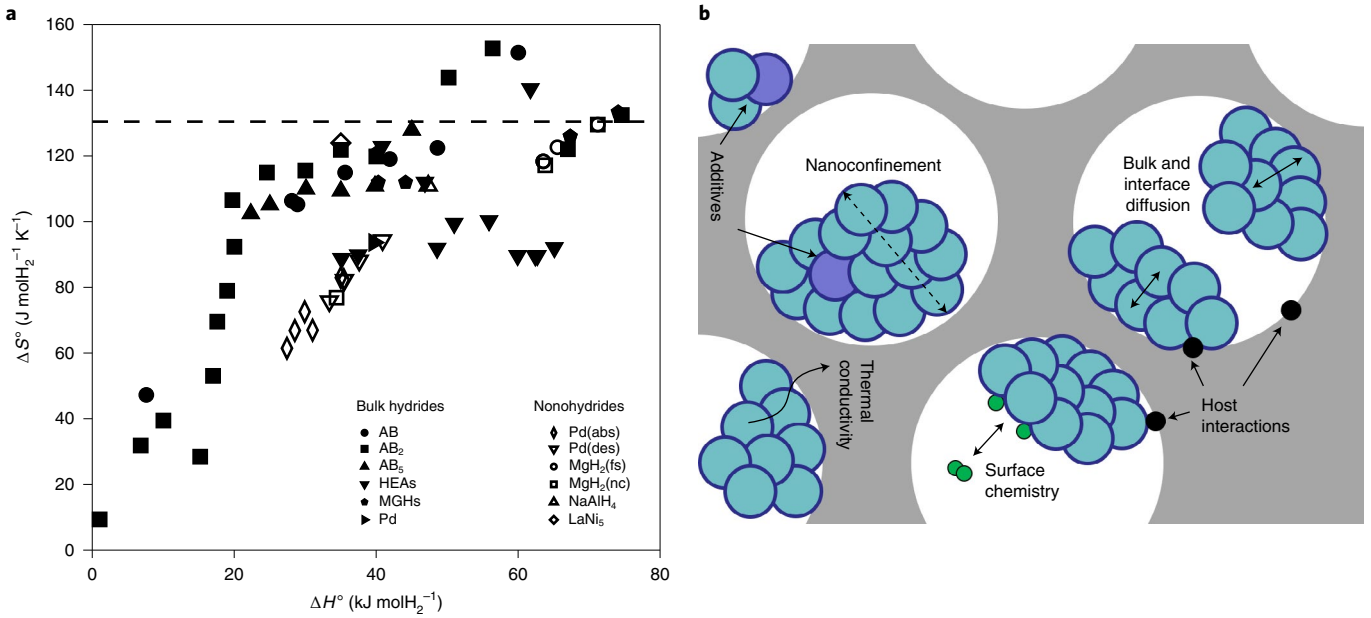

Fig. 3 | Nanoconfinement of metal hydrides produces a variety of effects that can cause Δ*H*° and Δ*S*° to be correlated. a, Trends in Δ*S*° versus Δ*H*° of bulk metal hydrides (solid symbols) are difficult to discern and vary relatively little if $\Delta H° \geq 20$ kJ $molH_2^{-1}$. In contrast, nanoscale hydrides (open symbols) exhibit a fairly strong entropy–enthalpy correlation (also see Extended Data Fig. 1). Metal hydride entropies are often assumed to be equal to that of H_2 gas (130.5 J $molH_2^{-1}$ K^{-1}; horizontal dashed line), but measured values[16] (Supplementary Table 1) show that this is rarely the case. HEAs, high-entropy alloys; MGHs, main-group hydrides; MgH_2(fs), free-standing magnesium hydride nanoparticles; MgH_2(nc), nanoconfined magnesium hydride. AB, interstitial hydride with A and B sites; Pd(abs), thermodynamics for hydrogen absorption by palladium; Pd(des), thermodynamics for hydrogen desorption by Pd. **b**, During nanoconfinement of metal hydrides (turquoise circles) within a porous host (grey), a decreasing nanoparticle diameter (dashed double arrow) reduces the surface-to-volume ratio, which alters the thermodynamics and kinetics of hydrogen release and uptake. Acceleration of bulk hydride reaction kinetics by compounds such as metal halides (additives; purple circles) is sometimes observed at the nanoscale. During host interactions, porous host materials with electron-donating or accepting groups (black circles) can reduce the mobility (and thus agglomeration) and modify the reactivity of metal hydrides via charge transfer interactions. Surface entropy and disorder, as well as defects and impurities or oxidation (surface chemistry), all have documented effects on H_2 (green circles) reactivity and kinetics[16]. The host can also accelerate reactions by transporting heat more efficiently than the bulk material (thermal conductivity).

and homogeneous catalysts. Using Mg-MOF-74 to support undercoordinated Ni^{2+} sites produced a catalyst that dehydrogenates alcohols at rates comparable to Raney nickel[50]. Intriguingly, several Mg MOFs with the IRMOF-74 topology also catalyse the hydrogenolysis of aryl ethers[51], suggesting the possibility for reversible dehydrogenation.

Metal hydrides

Trade-offs between H_2 release thermodynamics and reversible capacity are the primary factors when considering metal hydrides for transportation, where minimizing storage system volume and weight are paramount. For stationary applications, gravimetric capacity is less of a concern, but the high usage requirements (Table 1) suggest that volumetric capacity will remain important. Metal hydrides excel here; their volumetric capacity is at least double 700-bar pressurized gas. However, those with the highest gravimetric capacities (Supplementary Table 1) also exhibit slow dehydrogenation rates due to strong M–H bonding (Fig. 2)[16,52–64]. For example, $LiBH_4$ has a high gravimetric capacity (13.9 wt%H) but a very high Δ*H*° (72 kJ $molH_2^{-1}$ at 298 K). Alternatively, interstitial hydrides have much lower Δ*H*° but low gravimetric capacity (for example, $TiFeH_2$: 1.91 wt%H). Complex metal hydrides lie thermodynamically between ionic and interstitial hydrides, but nucleation, mass transport or kinetic bottlenecks in borohydrides, amides and alanates arise due to their multistep dehydrogenation mechanisms[15,16,65–67].

One strategy to surmount this challenge is to maximize Δ*S*° while minimizing Δ*H*°. Metal hydride thermodynamics are governed by the van't Hoff equation:

$$\ln[p_{eq}] = -\frac{\Delta H°}{RT} + \frac{\Delta S°}{R} \quad (1)$$

where p_{eq} is the equilibrium vapor pressure of H_2, *R* is the gas constant, and *T* is the temperature. The extent to which Δ*H*° and Δ*S*° can be independently controlled is unclear[65,66,68,69]. The modulation of Δ*H*° appears more straightforward using new approaches such as eutectic melting[70], microstructure-induced strain[71], high-entropy metal alloying[72] and compositional tuning[73]. However, strategies to independently tune Δ*S*° have not been demonstrated[16,65]. These may be needed to reduce entropy–enthalpy compensation, in which decreasing Δ*H*° is counteracted by a smaller Δ*S*°[71,74,75]. Encouragingly, we recently found using a machine learning model that Δ*S*° of high-entropy alloys is related to the corresponding volume change[72]. The material features in this model that best predicted Δ*H*° differ from those for Δ*S*°[10,72]. Coupling this result with the lack of a clear entropy–enthalpy correlation for several hydride classes (Fig. 3a and Extended Data Fig. 1) suggests that independent Δ*S*° tuning should be possible.

Another challenge for bulk metal hydrides is controlling hydrogen release and uptake kinetics. For complex metal hydrides, these seldom occur via a single-step mechanism. Two recent investigations demonstrate the controlling role that surface and internal interfaces play. First, in contrast with previous assumptions, the thin oxide layer on the surface of $NaAlH_4$ particles actually facilitates H_2 release rather than impeding it[76]. Second, scanning transmission X-ray microscopy images of partially dehydrogenated $LiNH_2$ particles reveal core-shell structures that could only form if H_2 release is limited by surface desorption, rather than internal hydrogen mass transport[21]. These conclusions represent a radical departure from the conventional understanding of metal hydride reaction chemistry, motivating a reassessment of metal hydride kinetics mechanisms, even for well-studied materials such as Ti-doped $NaAlH_4$[77].

https://doi.org/10.1038/s41557-022-01056-2

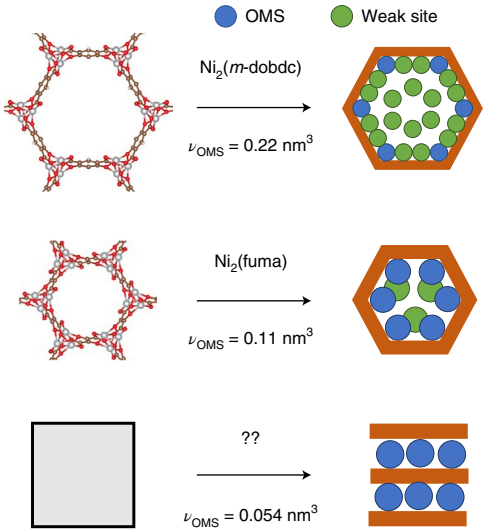

Fig. 4 | High open metal site density MOFs. Schematic of Ni_2(*m*-dobdc), computationally predicted Ni_2(fuma) and an unknown, hypothetical material (shown as a grey square) with different ratios of OMSs and weak sites and different v_{OMS} values (C, brown; O, red; Ni, grey). Adsorption sites at OMSs and weak sites are represented by blue and green circles, respectively. Exceptionally low v_{OMS} MOFs such as the hypothetical material would provide the best chances of reaching the ultimate DOE storage targets, yet still must exhibit the narrowly optimal hydrogen-binding energy range. While large binding energies decrease the usable capacity under all conditions in rigid MOFs, this could be circumvented in the future via flexible MOFs that undergo a nonporous-to-porous transition that is stabilized by strong hydrogen–OMS interactions.

Nanoscaling to increase surface energies, destabilize intermediates and eliminate difficult-to-control microstructural effects is a promising strategy for overcoming the limitations of bulk metal hydrides (Fig. 3b)[16]. Recent computational modelling suggests that beyond-ideal effects should be explored to optimize nanoparticle properties, including surface anharmonic dynamics, interface and surface energy penalties, mechanical stress, surface oxides/hydroxides and disordered phases[78]. However, a problem can arise if entropy–enthalpy compensation occurs. Entropic effects are observed for nanoscale MgH_2[54], PdH_x[79] and $LaNi_5$[80], but thermodynamics data for most other nanoscale hydrides are too limited to assess their importance (Fig. 3a). However, our statistical analysis of the available nanohydride data[16] suggests that $\Delta S°$ and $\Delta H°$ are correlated for MgH_2 and PdH_x (Extended Data Fig. 1).

Uncoupling $\Delta S°$ of nanohydrides from $\Delta H°$ may be possible using material formats that strongly immobilize nanoclusters, thereby lowering $S°_{nanocluster}$ and increasing $\Delta S°$. Assuming a nanocluster is least mobile when locked in the bulk crystal structure, $S°_{nanocluster}$ increases with increasing mismatch between host size and decreasing host–nanocluster interaction. Data for MgH_2 support this strategy: $\Delta S°$ for bulk[75] > 7-nm ball-milled[75] > reduced graphene oxide-encapsulated (3–4 nm)[71] > infiltrated porous carbon (<3 nm)[81] (133.4, 129.6, 126.3 and 117.2 J molH_2^{-1} K^{-1}, respectively). Alternatively, if a metastable metal hydride such as $LiAlH_4$ or AlH_3 could be thermodynamically stabilized, the increased $\Delta H°$ could offset a low $\Delta S°$. We recently achieved this for $LiAlH_4$ and AlH_3 using, respectively, nitrogen-doped ordered mesoporous carbon (N-doped CMK-3)[82] and a bipyridine-functionalized covalent triazine framework as supports[83]. Surprisingly, hydrogen release is reversible in both cases.

A second, largely overlooked aspect of nanoscaling is the dependence of maximum usable capacity on particle size (the usable capacity is the difference in hydrogen uptake between the absorption and desorption conditions). As seen in a number of cases[16], nanoconfinement can change the behaviour of metal hydride particles compared with both the free-standing counterpart and the bulk as a result of non-innocent hosts that exhibit charge transfer with the hydride (Fig. 3b). Consequently, tuning the size and composition of confined hydride nanoparticles could be a useful tool for maximizing usable capacity. This effect needs to be carefully assessed by comparing the uptake of nanoconfined and free-standing particles for a range of both hydrides and host types so that design principles can be determined.

Sorbents

Extensive research on adsorbent materials has revealed that isosteric heats of adsorption (Fig. 2) are typically too low for non-cryogenic onboard vehicular storage[84,85], but may not be a barrier for stationary applications such as refuelling stations[86] (Table 1) or applications where the disadvantages of compressed gas or liquid H_2 are prohibitive[87]. Improved thermodynamics can be achieved by incorporating strong binding sites, yet no existing materials have sufficient volumetric density of these to meet the demanding DOE targets for light-duty vehicles. Even with plentiful chemisorption sites having optimal thermodynamics, inaccessible capacity in the 0–5 bar range remains problematic for fuel cell-related use cases[88]. Thus, a trifecta of fundamental chemistry challenges arises that must be surmounted to meet the requirements of many gas storage applications[5].

Currently, the only adsorbents with sufficient design versatility are MOFs, particularly those with exposed charge density at undercoordinated open metal sites (OMSs) that interact strongly with H_2[89]. For example, Ni_2(*m*-dobdc) (where *m*-dobdc = 4,6-dioxido-1,3-benzenedicarboxylate), which has a favourably low crystallographic volume per OMS ($v_{OMS} \approx 0.22$ nm^3) and isosteric heat of adsorption (q_{st} = 12.3 kJ mol^{-1}), provides the current record usable capacity (11.9 g l^{-1}; 5↔100 bar pressure swing at 298 K)[24,90]. Even lower $v_{OMS} \approx 0.11$ nm^3 could be achieved if the computationally predicted Ni_2(fuma) (where fuma = 2,3-dihydroxyfumarate) analogue can be synthesized[91]. Alternatively, Cu^I-MFU-4*l* (post-synthetic replacement of Zn^{II}-Cl with Cu^I in [Zn_5Cl_4(BTDD)$_3$], where BTDD is bis(1*H*-1,2,3-triazolo[4,5-*b*],[4′,5′-*i*])dibenzo[1,4]dioxin)) exhibits a remarkably high q_{st} (32 kJ mol^{-1})[92] but this is offset by high v_{OMS} (0.77 nm^3). Unfortunately, only one known MOF has the optimal binding strength, but again its v_{OMS} is too large[93,94]. This begs the question: 'Can DOE targets be met solely by minimizing v_{OMS} and optimizing q_{st} in a yet-to-be-identified material?'.

Insight can be gained from a multi-site Langmuir adsorption analysis[95], which can predict the quantity of adsorbed hydrogen, and thus the usable capacity, as a function of the pressure, temperature and binding site energies in rigid materials. An optimal heat of adsorption ($\approx 15 < q_{st} < 20$ kJ mol^{-1}) in rigid materials is a necessary but insufficient criterion for high usable capacity, since low v_{OMS} is simultaneously required to maximize the deliverable capacity. Structures with decreasing v_{OMS} are illustrated through Ni_2(*m*-dobdc), Ni_2(fuma) and a hypothetical material with a very high density of OMSs (Fig. 4). Both Ni_2(*m*-dobdc) and Ni_2(fuma) have q_{st} below the optimal range; furthermore, even if q_{st} could be increased into the optimal range in these particular frameworks (for example, by substituting the metal for one with a stronger hydrogen-binding energy), their insufficiently low v_{OMS} values preclude them from reaching the ultimate DOE storage targets (50 gH_2 l^{-1}), regardless of how well any OMS would bind hydrogen.

The hypothetical material with an ultra-low v_{OMS} could still only achieve ultimate DOE targets (50 gH_2 l^{-1}) within a narrow binding energy range because simply increasing the binding strength at any given v_{OMS} universally leads to higher uptake under the desorption conditions, thereby reducing the usable capacity. This trade-off has been remedied in other gas storage applications through flexible nonporous-to-porous transitions[88,96]. Indeed, H_2-induced breathing is observed in the non-OMS Co(BDP) framework (where BDP is 1,4-benzenedi(4′-pyrazolyl))[97], but the weak H_2–framework interactions (estimated at around 2–8 kJ mol^{-1}) cannot stabilize the porous state above cryogenic

temperatures. We conclude that sorbent development efforts should target flexible materials with buried OMSs in the nonporous state and with strong (≥15 kJ mol^{-1}) OMS–H_2 interactions that facilitate a nonporous–porous transition closer to ambient temperature.

Data science and machine learning

Computational and machine learning approaches are playing an important role in predicting the properties of all of the material classes discussed above, including the capacity and thermodynamics of LOHCs[98] and various hydride and superhydride phases[10,99]. Nanoporous materials provide a clear illustration, as high-throughput screening has both elucidated their performance limits and identified promising candidates for various gas storage and separation applications[100–104]. Screening for H_2 physisorption has typically used either approximate correlations for estimating uptake[101] or Monte Carlo simulations[105–107] based on potentials such as the universal force field (UFF)[108]. This is necessary to make simulations of hundreds of thousands of materials computationally feasible. However, although the UFF is applicable across the periodic table, it does not accurately capture the potential energy surface of some chemical and structural motifs observed in MOFs[109–111]—a prime example being strong H_2 interactions with OMSs[112–114]. Moreover, most screening studies assumed cryogenic temperatures (77 K), favouring a high probability of H_2 occupation of weak physisorption sites and allowing materials lacking OMSs to still have very large volumetric uptake on par with the DOE targets. Consequently, although screening studies have been very useful for elucidating structure–property relationships and design trade-offs at cryogenic temperatures, it is unclear whether their results translate to near-ambient-temperature adsorption in MOFs with strong (open metal) binding sites. For example, the UFF accurately assesses MOF-5 as a high-capacity material at 77 K, even though it is much less useful in practice at non-cryogenic temperatures than Ni_2(*m*-dobdc), whose capacity at ambient temperature is not accurately predicted by the UFF. In other words, a MOF with 'Goldilocks' binding sites will be inaccurately assessed by high-throughput screening studies using off-the-shelf force fields, which were initially developed for other materials.

The most recent version of the Computation-Ready, Experimental (CoRE) MOF database[115], which automatically identifies MOFs with OMSs, sheds new light on the scope of this problem. Approximately 50% of all CoRE MOF structures contain OMSs (Supplementary Fig. 1), which in some cases constitute most if not all possible adsorption sites. Next-generation high-throughput screening studies will more accurately evaluate such materials through a variety of computational approaches. Density functional theory calculations are now regularly executed within high-throughput material property predictions[116–118] and have already been used for large-scale relaxation of MOF structures[119]. An important step forward, therefore, would be to relax at least a subset (several hundred) of MOFs with OMSs and to compute their H_2 binding energy. Statistical/machine learning techniques could then be used to construct a model of H_2 interactions that, at minimum, would provide higher accuracy than the UFF. Such concepts have already been used to screen other classes of hydrogen storage materials[10,120]. Atomistic machine learning potentials[121,122], which provide first-principles accuracy but are computationally more expensive than classical force field predictions, might eventually be used for direct simulation of hydrogen uptake by MOFs with OMSs, given recent substantial algorithmic improvements[123].

Conclusions and future directions

For years, hydrogen storage research focused primarily on light-duty vehicles, which is understandable given the large greenhouse gas emissions from this sector. The DOE targets for these vehicles[5] performed a valuable service by focusing research on the most critical issues. Unfortunately, this has led to an overemphasis on gravimetric capacity and enthalpy tuning to enable ambient-temperature storage or release using only the residual fuel cell heat. Another unanticipated consequence was that some material classes (for example, interstitial hydrides) were neglected. Encouragingly, materials that could not meet DOE targets for light-duty vehicles may prove to be ideal for other uses (Table 1), including MOFs with high capacity at low temperatures[124] and nanoscale hydrides with attractive thermodynamics compared with bulk[16].

In future efforts to develop materials-based storage, some established theories should be re-examined to identify strategies to overcome the challenges discussed above. First, ideal (that is, defect-free) X-ray crystal structures may be insufficient to describe material behaviours; examples include the nonporous-to-porous transitions discussed above and adaptive MOF pores[125]. A corollary is that surface chemistry, not bulk processes, may govern kinetic behaviour, as has been shown for some complex hydrides[21,76]. Second, the role of entropy cannot be neglected. For example, reversible hydrogen desorption by metastable hydrides (which was long thought to be infeasible) was recently achieved by nanoscaling[82,83], but will entropy–enthalpy compensation limit further improvements? Finally, in all cases, usable capacity—not the theoretical maximum uptake—is paramount. Although it is well recognized for sorbents, this is underappreciated for metal hydrides. Moreover, material design must consider other properties, such as heat transfer, to achieve the required dehydrogenation and refuelling rates. Fortunately, the ever-expanding hydrogen storage literature suggests that the challenges discussed here will be surmounted, enabling this technology to fulfil its vital role in a renewable energy economy.

References

1. Arbabzadeh, M., Sioshansi, R., Johnson, J. X. & Keoleian, G. A. The role of energy storage in deep decarbonization of electricity production. *Nat. Commun.* **10**, 3413 (2019).
2. *The Future of Hydrogen* (IEA, 2019).
3. Pivovar, B., Rustagi, N. & Satyapal, S. Hydrogen at scale (H_2@Scale): key to a clean, economic, and sustainable energy system. *Electrochem. Soc. Interface* **27**, 47–52 (2018).
4. *The National Hydrogen Strategy* (Federal Ministry for Economic Affairs and Climate Action, 2020).
5. *Target Explanation Document: Onboard Hydrogen Storage for Light-Duty Fuel Cell Vehicles* (US DOE, 2017).
6. Ahluwalia, R. K. et al. Technical assessment of cryo-compressed hydrogen storage tank systems for automotive applications. *Int. J. Hydrog. Energy* **35**, 4171–4184 (2010).
7. Allendorf, M. D. et al. An assessment of strategies for the development of solid-state adsorbents for vehicular hydrogen storage. *Energy Environ. Sci.* **11**, 2784–2812 (2018).
8. Pasini, J. M. et al. Metal hydride material requirements for automotive hydrogen storage systems. *Int. J. Hydrog. Energy* **38**, 9755–9765 (2013).
9. Bhatia, S. K. & Myers, A. L. Optimum conditions for adsorptive storage. *Langmuir* **22**, 1688–1700 (2006).
10. Witman, M. et al. Extracting an empirical intermetallic hydride design principle from limited data via interpretable machine learning. *J. Phys. Chem. Lett.* **11**, 40–47 (2020).
11. Grubel, K., Jeong, H., Yoon, C. W. & Autrey, T. Challenges and opportunities for using formate to store, transport, and use hydrogen. *J. Energy Chem.* **41**, 216–224 (2020).
12. Zou, Y.-Q., von Wolff, N., Anaby, A., Xie, Y. & Milstein, D. Ethylene glycol as an efficient and reversible liquid–organic hydrogen carrier. *Nat. Catal.* **2**, 415–422 (2019).
13. Zhu, Q. L. & Xu, Q. Liquid organic and inorganic chemical hydrides for high-capacity hydrogen storage. *Energy Environ. Sci.* **8**, 478–512 (2015).
14. Preuster, P., Papp, C. & Wasserscheid, P. Liquid organic hydrogen carriers (LOHCs): toward a hydrogen-free hydrogen economy. *Acc. Chem. Res.* **50**, 74–85 (2017).

15. Mohtadi, R. & Orimo, S.-i The renaissance of hydrides as energy materials. *Nat. Rev. Mater.* **2**, 16091 (2017).
16. Schneemann, A. et al. Nanostructured metal hydrides for hydrogen storage. *Chem. Rev.* **118**, 10775–10839 (2018).
17. Chen, L.-N. et al. Efficient hydrogen production from methanol using a single-site Pt_1/CeO_2 catalyst. *J. Am. Chem. Soc.* **141**, 17995–17999 (2019).
18. Sordakis, K. et al. Homogeneous catalysis for sustainable hydrogen storage in formic acid and alcohols. *Chem. Rev.* **118**, 372–433 (2018).
19. Onishi, N., Laurenczy, G., Beller, M. & Himeda, Y. Recent progress for reversible homogeneous catalytic hydrogen storage in formic acid and in methanol. *Coord. Chem. Rev.* **373**, 317–332 (2018).
20. Jeon, K. J. et al. Air-stable magnesium nanocomposites provide rapid and high-capacity hydrogen storage without using heavy-metal catalysts. *Nat. Mater.* **10**, 286–290 (2011).
21. White, J. L. et al. The inside-outs of metal hydride dehydrogenation: imaging the phase evolution of the Li-N-H hydrogen storage system. *Adv. Mater. Interfaces* **7**, 1901905 (2020).
22. Tsivion, E., Long, J. R. & Head-Gordon, M. Hydrogen physisorption on metal–organic framework linkers and metalated linkers: a computational study of the factors that control binding strength. *J. Am. Chem. Soc.* **136**, 17827–17835 (2014).
23. Runcevski, T. et al. Adsorption of two gas molecules at a single metal site in a metal–organic framework. *Chem. Commun.* **52**, 8251–8254 (2016).
24. Kapelewski, M. T. et al. Record high hydrogen storage capacity in the metal organic framework Ni_2(*m*-dobdc) at near-ambient temperatures. *Chem. Mater.* **30**, 8179–8189 (2018).
25. Jawahery, S. et al. Adsorbate-induced lattice deformation in IRMOF-74 series. *Nat. Commun.* **8**, 13945 (2017).
26. Witman, M. et al. The influence of intrinsic framework flexibility on adsorption in nanoporous materials. *J. Am. Chem. Soc.* **139**, 5547–5557 (2017).
27. Kanoo, P. et al. Pseudo-gated adsorption with negligible volume change evoked by halogen-bond interaction in the nanospace of MOFs. *Chem. Eur. J.* **26**, 2148–2153 (2020).
28. Moosavi, S. M. et al. Capturing chemical intuition in synthesis of metal–organic frameworks. *Nat. Commun.* **10**, 539 (2019).
29. Aaldto-Saksa, P. T., Cook, C., Kiviaho, J. & Repo, T. Liquid organic hydrogen carriers for transportation and storing of renewable energy—review and discussion. *J. Power Sources* **396**, 803–823 (2018).
30. Gianotti, E., Taillades-Jacquin, M., Roziere, J. & Jones, D. J. High-purity hydrogen generation via dehydrogenation of organic carriers: a review on the catalytic process. *ACS Catal.* **8**, 4660–4680 (2018).
31. Modisha, P. M., Ouma, C. N. M., Garidzirai, R., Wasserscheid, P. & Bessarabov, D. The prospect of hydrogen storage using liquid organic hydrogen carriers. *Energy Fuels* **33**, 2778–2796 (2019).
32. Niermann, M., Beckendorff, A., Kaltschmitt, M. & Bonhoff, K. Liquid organic hydrogen carrier (LOHC)—assessment based on chemical and economic properties. *Int. J. Hydrog. Energy* **44**, 6631–6654 (2019).
33. Clot, E., Eisenstein, O. & Crabtree, R. H.Computational structure-activity relationships in H_2 storage: how placement of N atoms affects release temperatures in organic liquid storage materials. *Chem. Commun.* **2007**, 2231–2233 (2007).
34. Cheng, H., Wu, J., Dong, Y. & Yang, M. Liquid hydrogen storage system. US patent 20180065849A1 (2015).
35. Verevkin, S. P., Konnova, M. E., Zherikova, K. V. & Pimerzin, A. A. Sustainable hydrogen storage: thermochemistry of amino-alcohols as seminal liquid organic hydrogen carriers. *J. Chem. Thermo.* **163**, 106591 (2021).
36. Tran, B. L., Johnson, S. I., Brooks, K. P. & Autrey, S. T. Ethanol as a liquid organic hydrogen carrier for seasonal microgrid application: catalysis, theory, and engineering feasibility. *ACS Sustain. Chem. Eng.* **9**, 7130–7138 (2021).
37. Onoda, M., Nagano, Y. & Fujita, K. Iridium-catalyzed dehydrogenative lactonization of 1,4-butanediol and reversal hydrogenation: new hydrogen storage system using cheap organic resources. *Int. J. Hydrog. Energy* **44**, 28514–28520 (2019).
38. Hu, P., Fogler, E., Diskin-Posner, Y., Iron, M. A. & Milstein, D. A novel liquid organic hydrogen carrier system based on catalytic peptide formation and hydrogenation. *Nat. Commun.* **6**, 6859 (2015).
39. Grubel, K. et al. Research requirements to move the bar forward using aqueous formate salts as H_2 carriers for energy storage applications. *J. Energy Power Technol.* **2**, 16 (2020).
40. Su, J., Lu, M. & Lin, H. F. High yield production of formate by hydrogenating CO_2 derived ammonium carbamate/carbonate at room temperature. *Green Chem.* **17**, 2769–2773 (2015).
41. Weisz, P. B. Diffusion and chemical transformation. *Science* **179**, 433–440 (1973).
42. Weisz, P. B.The science of the possible. *ChemTech* **12**, 424–425 (1982).
43. Peters, W. et al. Macrokinetic effects in perhydro-*N*-ethylcarbazole dehydrogenation and H_2 productivity optimization by using egg-shell catalysts. *Energy Environ. Sci.* **8**, 3013–3021 (2015).
44. Alhumaidan, F., Cresswell, D. & Garforth, A. Hydrogen storage in liquid organic hydride: producing hydrogen catalytically from methylcyclohexane. *Energy Fuels* **25**, 4217–4234 (2011).
45. Andersson, J. Application of liquid hydrogen carriers in hydrogen steelmaking. *Energies* **14**, 1392 (2021).
46. Yolcular, S. & Olgun, O. Ni/Al_2O_3 catalysts and their activity in dehydrogenation of methylcyclohexane for hydrogen production. *Catal. Today* **138**, 198–202 (2008).
47. Al-ShaikhAli, A. H., Jedidi, A., Cavallo, L. & Takanabe, K. Non-precious bimetallic catalysts for selective dehydrogenation of an organic chemical hydride system. *Chem. Commun.* **51**, 12931–12934 (2015).
48. Yamaguchi, R., Ikeda, C., Takahashi, Y. & Fujita, K. Homogeneous catalytic system for reversible dehydrogenation–hydrogenation reactions of nitrogen heterocycles with reversible interconversion of catalytic species. *J. Am. Chem. Soc.* **131**, 8410–8412 (2009).
49. Hu, P., Ben-David, Y. & Milstein, D. Rechargeable hydrogen storage system based on the dehydrogenative coupling of ethylenediamine with ethanol. *Angew. Chem. Int. Ed.* **55**, 1061–1064 (2016).
50. Snider, J. L. et al. Stabilized open metal sites in bimetallic metal–organic framework catalysts for hydrogen production from alcohols. *J. Mater. Chem. A* **9**, 10869–10881 (2021).
51. Stavila, V. et al. IRMOF-74(*n*)–Mg: a novel catalyst series for hydrogen activation and hydrogenolysis of C–O bonds. *Chem. Sci.* **10**, 9880–9892 (2019).
52. Gu, T. T., Gu, J., Zhang, Y. & Ren, H. Metal borohydride-based system for solid-state hydrogen storage. *Prog. Chem.* **32**, 665–686 (2020).
53. Li, B., Li, J. D., Zhao, H. J., Yu, X. Q. & Shao, H. Y. Mg-based metastable nano alloys for hydrogen storage. *Int. J. Hydrog. Energy* **44**, 6007–6018 (2019).
54. Sun, Y. H. et al. Tailoring magnesium based materials for hydrogen storage through synthesis: current state of the art. *Energy Storage Mater.* **10**, 168–198 (2018).
55. Li, J. D., Li, B., Shao, H. Y., Li, W. & Lin, H. J. Catalysis and downsizing in Mg-based hydrogen storage materials. *Catalysts* **8**, 89 (2018).
56. Yu, X. B., Tang, Z. W., Sun, D. L., Ouyang, L. Z. & Zhu, M. Recent advances and remaining challenges of nanostructured materials for hydrogen storage applications. *Prog. Mater Sci.* **88**, 1–48 (2017).

57. Rusman, N. A. A. & Dahari, M. A review on the current progress of metal hydrides material for solid-state hydrogen storage applications. *Int. J. Hydrog. Energy* **41**, 12108–12126 (2016).
58. Niaz, S., Manzoor, T. & Pandith, A. H. Hydrogen storage: materials, methods and perspectives. *Renew. Sustain. Energy Rev.* **50**, 457–469 (2015).
59. Møller, K. T. et al. Complex metal hydrides for hydrogen, thermal and electrochemical energy storage. *Energies* **10**, 1645 (2017).
60. Paskevicius, M. et al. Metal borohydrides and derivatives—synthesis, structure and properties. *Chem. Soc. Rev.* **46**, 1565–1634 (2017).
61. Xiong, Z. T., Wu, G. T., Hu, H. J. & Chen, P. Ternary imides for hydrogen storage. *Adv. Mater.* **16**, 1522–1525 (2004).
62. Luo, W. F.($LiNH_2$-MgH_2): a viable hydrogen storage system. *J. Alloys Compd.* **381**, 284–287 (2004).
63. Lu, J., Fang, Z. Z. G., Choi, Y. J. & Sohn, H. Y. Potential of binary lithium magnesium nitride for hydrogen storage applications. *J. Phys. Chem. C* **111**, 12129–12134 (2007).
64. Wang, J. et al. Potassium-modified $Mg(NH_2)_2$/2 LiH system for hydrogen storage. *Angew. Chem. Int. Ed.* **48**, 5828–5832 (2009).
65. He, T., Cao, H. J. & Chen, P. Complex hydrides for energy storage, conversion, and utilization. *Adv. Mater.* **31**, 1902757 (2019).
66. Liu, X., Wu, C., Wu, F. & Bai, Y. Light metal complex hydride hydrogen storage systems. *Prog. Chem.* **27**, 1167–1181 (2015).
67. Orimo, S. I., Nakamori, Y., Eliseo, J. R., Zuttel, A. & Jensen, C. M. Complex hydrides for hydrogen storage. *Chem. Rev.* **107**, 4111–4132 (2007).
68. Ouyang, L., Chen, K., Jiang, J., Yang, X.-S. & Zhu, M. Hydrogen storage in light-metal based systems: a review. *J. Alloys Compd.* **829**, 154597 (2020).
69. Berube, V., Radtke, G., Dresselhaus, M. & Chen, G. Size effects on the hydrogen storage properties of nanostructured metal hydrides: a review. *Int. J. Energy Res.* **31**, 637–663 (2007).
70. Pal, P., Jain, A., Miyaoka, H., Kojima, Y. & Ichikawa, T. Eutectic melting in *x*($2LiBH_4$-MgH_2) hydrogen storage system by the addition of KH. *Int. J. Hydrog. Energy* **45**, 17000–17005 (2020).
71. Cho, E. S. et al. Hierarchically controlled inside-out doping of Mg nanocomposites for moderate temperature hydrogen storage. *Adv. Funct. Mater.* **27**, 1704316 (2017).
72. Witman, M. et al. Data-driven discovery and synthesis of high entropy alloy hydrides with targeted thermodynamic stability. *Chem. Mater.* **33**, 4067–4076 (2021).
73. Pinkerton, F. E., Meyer, M. S., Meisner, G. P., Balogh, M. P. & Vajo, J. J. Phase boundaries and reversibility of $LiBH_4$/MgH_2 hydrogen storage material. *J. Phys. Chem. C* **111**, 12881–12885 (2007).
74. Lohstroh, W., Roth, A., Hahn, H. & Fichtner, M. Thermodynamic effects in nanoscale $NaAlH_4$. *ChemPhysChem* **11**, 789–792 (2010).
75. Paskevicius, M., Sheppard, D. A. & Buckley, C. E. Thermodynamic changes in mechanochemically synthesized magnesium hydride nanoparticles. *J. Am. Chem. Soc.* **132**, 5077–5083 (2010).
76. White, J. L. et al. Identifying the role of dynamic surface hydroxides in the dehydrogenation of Ti-doped $NaAlH_4$. *ACS Appl. Mater. Interfaces* **11**, 4930–4941 (2019).
77. Frankcombe, T. J. Proposed mechanisms for the catalytic activity of Ti in $NaAlH_4$. *Chem. Rev.* **112**, 2164–2178 (2012).
78. Wood, B. C., Heo, T. W., Kang, S., Wan, L. F. & Li, S. Beyond idealized models of nanoscale metal hydrides for hydrogen storage. *Ind. Eng. Chem. Res.* **59**, 5786–5796 (2020).
79. Griessen, R., Strohfeldt, N. & Giessen, H. Thermodynamics of the hybrid interaction of hydrogen with palladium nanoparticles. *Nat. Mater.* **15**, 311–317 (2016).
80. Liu, W. & Aguey-Zinsou, K.-F. Synthesis of highly dispersed nanosized $LaNi_5$ on carbon: revisiting particle size effects on hydrogen storage properties. *Int. J. Hydrog. Energy* **41**, 14429–14436 (2016).
81. Zhao-Karger, Z. et al. Altered thermodynamic and kinetic properties of MgH_2 infiltrated in microporous scaffold. *Chem. Commun.* **46**, 8353–8355 (2010).
82. Cho, Y. et al. Reversing the irreversible: thermodynamic stabilization of $LiAlH_4$ nanoconfined within a nitrogen-doped carbon host. *ACS Nano* **15**, 10163–10174 (2021).
83. Stavila, V. et al. Defying thermodynamics: stabilization of alane within covalent triazine frameworks for reversible hydrogen storage. *Angew. Chem. Int. Ed.* **60**, 25815–25824 (2021).
84. Rosi, N. L. Hydrogen storage in microporous metal–organic frameworks. *Science* **300**, 1127–1129 (2003).
85. Murray, L. J., Dinca, M. & Long, J. R. Hydrogen storage in metal–organic frameworks. *Chem. Soc. Rev.* **38**, 1294 (2009).
86. Anastasopoulou, A. et al. Technoeconomic analysis of metal–organic frameworks for bulk hydrogen transportation. *Energy Environ. Sci.* **14**, 1083–1094 (2021).
87. Yang, C. & Ogden, J. Determining the lowest-cost hydrogen delivery mode. *Int. J. Hydrog. Energy* **32**, 268–286 (2007).
88. Witman, M. et al. Design principles for the ultimate gas deliverable capacity material: nonporous to porous deformations without volume change. *Mol. Syst. Des. Eng.* **5**, 1491–1503 (2020).
89. Kalmutzki, M. J., Hanikel, N. & Yaghi, O. M. Secondary building units as the turning point in the development of the reticular chemistry of MOFs. *Sci. Adv.* **4**, eaat9180 (2018).
90. Kapelewski, M. T. et al. M_2(*m*-dobdc) (M = Mg, Mn, Fe, Co, Ni) metal–organic frameworks exhibiting increased charge density and enhanced H_2 binding at the open metal sites. *J. Am. Chem. Soc.* **2**, 12119–12129 (2014).
91. Witman, M. et al. Rational design of a low-cost, high-performance metal–organic framework for hydrogen storage and carbon capture. *J. Phys. Chem. C* **121**, 1171–1181 (2017).
92. Denysenko, D., Grzywa, M., Jelic, J., Reuter, K. & Volkmer, D. Scorpionate-type coordination in MFU-4*l* metal–organic frameworks: small-molecule binding and activation upon the thermally activated formation of open metal sites. *Angew. Chem. Int. Ed.* **53**, 5832–5836 (2014).
93. Jaramillo, D. E. et al. Ambient-temperature hydrogen storage via vanadium(II)–dihydrogen complexation in a metal–organic framework. *J. Am. Chem. Soc.* **143**, 6248–6256 (2021).
94. Jaramillo, D. E. et al. Selective nitrogen adsorption via backbonding in a metal–organic framework with exposed vanadium sites. *Nat. Mater.* **19**, 517–521 (2020).
95. Simon, C. M. et al. Optimizing nanoporous materials for gas storage. *Phys. Chem. Chem. Phys.* **16**, 5499 (2014).
96. Kitagawa, S., Kitaura, R. & Noro, S.-I. Functional porous coordination polymers. *Angew. Chem. Int. Ed.* **43**, 2334–2375 (2004).
97. Choi, H. J., Dincă, M. & Long, J. R. Broadly hysteretic H_2 adsorption in the microporous metal–organic framework Co(1,4-benzenedipyrazolate). *J. Am. Chem. Soc.* **130**, 7848–7850 (2008).
98. Paragian, K., Li, B., Massino, M. & Rangarajan, S. A computational workflow to discover novel liquid organic hydrogen carriers and their dehydrogenation routes. *Mol. Syst. Des. Eng.* **5**, 1658–1670 (2020).
99. Hutcheon, M. J., Shipley, A. M. & Needs, R. J. Predicting novel superconducting hydrides using machine learning approaches. *Phys. Rev. B* **101**, 144505 (2020).
100. Banerjee, D. et al. Metal–organic framework with optimally selective xenon adsorption and separation. *Nat. Commun.* **7**, ncomms11831 (2016).
101. Goldsmith, J., Wong-Foy, A. G., Cafarella, M. J. & Siegel, D. J. Theoretical limits of hydrogen storage in metal–organic frameworks: opportunities and trade-offs. *Chem. Mater.* **25**, 3373–3382 (2013).

102. Gomez-Gualdron, D. A., Wilmer, C. E., Farha, O. K., Hupp, J. T. & Snurr, R. Q. Exploring the limits of methane storage and delivery in nanoporous materials. *J. Phys. Chem. C* **118**, 6941–6951 (2014).
103. Simon, C. M. et al. The materials genome in action: identifying the performance limits for methane storage. *Energy Environ. Sci.* **8**, 1190–1199 (2015).
104. Simon, C. M., Mercado, R., Schnell, S. K., Smit, B. & Haranczyk, M. What are the best materials to separate a xenon/krypton mixture? *Chem. Mater.* **27**, 4459–4475 (2015).
105. Ahmed, A. et al. Exceptional hydrogen storage achieved by screening nearly half a million metal–organic frameworks. *Nat. Commun.* **10**, 1568 (2019).
106. Bobbitt, N. S., Chen, J. & Snurr, R. Q. High-throughput screening of metal–organic frameworks for hydrogen storage at cryogenic temperature. *J. Phys. Chem. C* **120**, 27328–27341 (2016).
107. Thornton, A. W. et al. Materials genome in action: identifying the performance limits of physical hydrogen storage. *Chem. Mater.* **29**, 2844–2854 (2017).
108. Rappe, A. K., Casewit, C. J., Colwell, K. S., Goddard, W. A. & Skiff, W. M. UFF, a full periodic table force field for molecular mechanics and molecular dynamics simulations. *J. Am. Chem. Soc.* **114**, 10024–10035 (1992).
109. Dzubak, A. L. et al. Ab initio carbon capture in open-site metal–organic frameworks. *Nat. Chem.* **4**, 810–816 (2012).
110. Lee, K., Howe, J. D., Lin, L.-C., Smit, B. & Neaton, J. B. Small-molecule adsorption in open-site metal–organic frameworks: a systematic density functional theory study for rational design. *Chem. Mater.* **27**, 668–678 (2015).
111. Lin, L.-C., Lee, K., Gagliardi, L., Neaton, J. B. & Smit, B. Force-field development from electronic structure calculations with periodic boundary conditions: applications to gaseous adsorption and transport in metal–organic frameworks. *J. Chem. Theory Comput.* **10**, 1477–1488 (2014).
112. Pham, T. et al. Understanding the H_2 sorption trends in the M-MOF-74 series (M = Mg, Ni, Co, Zn). *J. Phys. Chem. C* **119**, 1078–1090 (2015).
113. Pham, T., Forrest, K. A., McLaughlin, K., Eckert, J. & Space, B. Capturing the H_2–metal interaction in Mg-MOF-74 using classical polarization. *J. Phys. Chem. C* **118**, 22683–22690 (2014).
114. Pham, T. et al. Simulations of hydrogen sorption in *rht*-MOF-1: identifying the binding sites through explicit polarization and quantum rotation calculations. *J. Mater. Chem. A* **2**, 2088–2100 (2014).
115. Chung, Y. G. et al. Advances, updates, and analytics for the computation-ready, experimental metal–organic framework database: CoRE MOF 2019. *J. Chem. Eng. Data* **64**, 5985–5998 (2019).
116. Alapati, S. V., Johnson, J. K. & Sholl, D. S. Identification of destabilized metal hydrides for hydrogen storage using first principles calculations. *J. Phys. Chem. B* **110**, 8769–8776 (2006).
117. Jain, A. et al. Commentary: the Materials Project: a materials genome approach to accelerating materials innovation. *APL Mater.* **1**, 011002 (2013).
118. Saal, J. E., Kirklin, S., Aykol, M., Meredig, B. & Wolverton, C. Materials design and discovery with high-throughput density functional theory: the Open Quantum Materials Database (OQMD). *JOM* **65**, 1501–1509 (2013).
119. Nazarian, D., Ganesh, P. & Sholl, D. S. Benchmarking density functional theory predictions of framework structures and properties in a chemically diverse test set of metal–organic frameworks. *J. Mater. Chem. A* **3**, 22432–22440 (2015).
120. Hattrick-Simpers, J. R., Choudhary, K. & Corgnale, C. A simple constrained machine learning model for predicting high-pressure-hydrogen-compressor materials. *Mol. Syst. Des. Eng.* **3**, 509–517 (2018).
121. Bartok, A. P., Payne, M. C., Kondor, R. & Csanyi, G. Gaussian approximation potentials: the accuracy of quantum mechanics, without the electrons. *Phys. Rev. Lett.* **104**, 136403 (2010).
122. Behler, J. & Parrinello, M. Generalized neural-network representation of high-dimensional potential-energy surfaces. *Phys. Rev. Lett.* **98**, 146401 (2007).
123. Jinnouchi, R., Lahnsteiner, J., Karsai, F., Kresse, G. & Bokdam, M. Phase transitions of hybrid perovskites simulated by machine-learning force fields trained on the fly with Bayesian inference. *Phys. Rev. Lett.* **122**, 225701 (2019).
124. Suh, M. P., Park, H. J., Prasad, T. K. & Lim, D.-W. Hydrogen storage in metal–organic frameworks. *Chem. Rev.* **112**, 782–835 (2012).
125. Allendorf, M. D., Stavila, V., Witman, M., Brozek, C. K. & Hendon, C. H. What lies beneath a metal–organic framework crystal structure? New design principles from unexpected behaviors. *J. Am. Chem. Soc.* **143**, 6705–6723 (2021).
126. *Technology Roadmap—Hydrogen and Fuel Cells* (IEA, 2015).
127. Cao, W., Zhang, J. & Li, H. Batteries with high theoretical energy densities. *Energy Storage Mater.* **26**, 46–55 (2020).
128. May, G. J., Davidson, A. & Monahov, B. Lead batteries for utility energy storage: a review. *J. Energy Storage* **15**, 145–157 (2018).
129. Pasquini, L. Design of nanomaterials for hydrogen storage. *Energies* **13**, 3503 (2020).
130. Klebanoff, L. E. *Hydrogen Storage Technology: Materials and Applications* (CRC Press, 2013).
131. Chen, P., Xiong, Z., Luo, J., Lin, J. & Tan, K. L. Interaction of hydrogen with metal nitrides and imides. *Nature* **420**, 302–304 (2002).
132. Ding, Z. et al. $LiBH_4$ for hydrogen storage—new perspectives. *Nano Mater. Sci.* **2**, 109–119 (2020).
133. Liu, M. et al. Novel 1D carbon nanotubes uniformly wrapped nanoscale MgH_2 for efficient hydrogen storage cycling performances with extreme high gravimetric and volumetric capacities. *Nano Energy* **61**, 540–549 (2019).
134. Von Colbe, J. B. et al. Application of hydrides in hydrogen storage and compression: achievements, outlook and perspectives. *Int. J. Hydrog. Energy* **44**, 7780–7808 (2019).
135. Zavorotynska, O., El-Kharbachi, A., Deledda, S. & Hauback, B. C. Recent progress in magnesium borohydride $Mg(BH_4)_2$: fundamentals and applications for energy storage. *Int. J. Hydrog. Energy* **41**, 14387–14403 (2016).
136. Zidan, R. et al. Aluminium hydride: a reversible material for hydrogen storage. *Chem. Commun.* **2009**, 3717–3719 (2009).
137. *Hydrogen and Fuel Cell Technologies Office Multi-Year Research, Development, and Demonstration Plan* Section 3.3 (Hydrogen and Fuel Cell Technologies Office, 2015).
138. Brooks, K. P., Semelsberger, T. A., Simmons, K. L. & van Hassel, B. Slurry-based chemical hydrogen storage systems for automotive fuel cell applications. *J. Power Sources* **268**, 950–959 (2014).
139. Tamburello, D., Hardy, B., Corgnale, C., Sulic, M. & Anton, D. Cryo-adsorbent hydrogen storage systems for fuel cell vehicles. In *Proc. ASME 2017 Fluids Engineering Division Summer Meeting* (American Society of Mechanical Engineers, 2017).
140. Bartscher, W., Rebizant, J. & Haschke, J. M. Equilibria and thermodynamic properties of the $ThZr_2{\cdot}H$ system. *J. Less Common Met.* **136**, 385–394 (1988).
141. Vajo, J. J., Mertens, F., Ahn, C. C., Bowman, R. C. & Fultz, B. Altering hydrogen storage properties by hydride destabilization through alloy formation: LiH and MgH_2 destabilized with Si. *J. Phys. Chem. B* **108**, 13977–13983 (2004).
142. Cahen, S., Eymery, J.-B., Janot, R. & Tarascon, J.-M. Improvement of the $LiBH_4$ hydrogen desorption by inclusion into mesoporous carbons. *J. Power Sources* **189**, 902–908 (2009).

143. Aakko-Saksa, P. T., Cook, C., Kiviaho, J. & Repo, T. Liquid organic hydrogen carriers for transportation and storing of renewable energy—review and discussion. *J. Power Sources* **396**, 803–823 (2018).
144. Sahlberg, M., Karlsson, D., Zlotea, C. & Jansson, U. Superior hydrogen storage in high entropy alloys. *Sci. Rep.* **6**, 36770 (2016).
145. Reilly, J. J. & Wiswall, R. H. Formation and properties of iron titanium hydride. *Inorg. Chem.* **13**, 218–222 (1974).
146. Marcinkoski, J. et al. *Hydrogen Class 8 Long Haul Truck Targets*. Report No. 19006 (Hydrogen and Fuel Cell Technologies Office, US DOE, 2019).
147. Brewer, E & Hanlin, J. *Fuel Cell Hybrid Electric Delivery Van Project*. In *2021 Annual Merit Review and Peer Evaluation Meeting* (Center for Transportation and the Environment, 2021); https://www.hydrogen.energy.gov/pdfs/review21/ta016_hanlin_2021_o.pdf
148. Pratt, J. W. & Klebanoff, L. E. *Feasibility of the SF-BREEZE: a Zero-Emission, Hydrogen Fuel Cell, High-Speed Passenger Ferry*. Report No. SAND2016-9719 (Sandia National Laboratories, 2016).
149. *FY 2018 Progress Report for the DOE Hydrogen and Fuel Cells Program*. Report No. DOE/GO-102019-5156 (US DOE, 2019).
150. Devlin, P. & Moreland, G. *Industry Deployed Fuel Cell Backup Power (BuP)*. Report No. 17004 (Hydrogen and Fuel Cell Technologies Office, US DOE, 2017).
151. Pauksztat, A., Saliger, R. & Boyanov, N. Residential energy supply concept with integration of renewable energies and energy storage. *Chem. Eng. Technol.* **42**, 1907–1913 (2019).
152. Kumagai, T. *AHEAD Launches Brunei–Japan Hydrogen Supply Chain for Power Generation in Tokyo Bay* (S&P Global, 2020).
153. *Energy Savings Analysis: ANSI/ASHRAE/IES Standard 90.1-2016* (Office of Energy Efficiency & Renewable Energy & US DOE, 2017).
154. Saur, G., Arjona, V., Clutterbuck, A. & Parker, E. *Hydrogen and Fuel Cells for Data Center Applications Project Meeting: Workshop Report* (National Renewable Energy Laboratory, 2019).
155. Mongird, K. et al. *2020 Grid Energy Storage Technology Cost and Performance Assessment*. Report No. DOE/PA-0204 (US DOE, 2020).

Acknowledgements

We gratefully acknowledge research support from the Hydrogen Materials Advanced Research Consortium (HyMARC), which was established as part of the Energy Materials Network under the US DOE Office of Energy Efficiency and Renewable Energy's Hydrogen and Fuel Cell Technologies Office, under contract numbers DE-AC04-94AL85000 and DE-AC52-07NA27344. Sandia National Laboratories is a multi-mission laboratory managed and operated by National Technology and Engineering Solutions of Sandia—a wholly owned subsidiary of Honeywell International—for the US DOE's National Nuclear Security Administration under contract DE-NA-0003525. The Pacific Northwest National Laboratory is operated by Battelle for the US DOE under contract DE-AC05-76RL01830.

Author contributions

M.D.A., V.S., M.W., J.L.S., T.A., M.E.B., K.B. and B.L.T. contributed to discussions and wrote the manuscript.

Competing interests

The authors declare no competing interests.

Additional information

Extended data is available for this paper at https://doi.org/10.1038/s41557-022-01056-2.

Supplementary information The online version contains supplementary material available at https://doi.org/10.1038/s41557-022-01056-2.

Correspondence should be addressed to Mark D. Allendorf or Mark E. Bowden.

Peer review information *Nature Chemistry* thanks the anonymous reviewers for their contribution to the peer review of this work.

https://doi.org/10.1038/s41557-022-01056-2

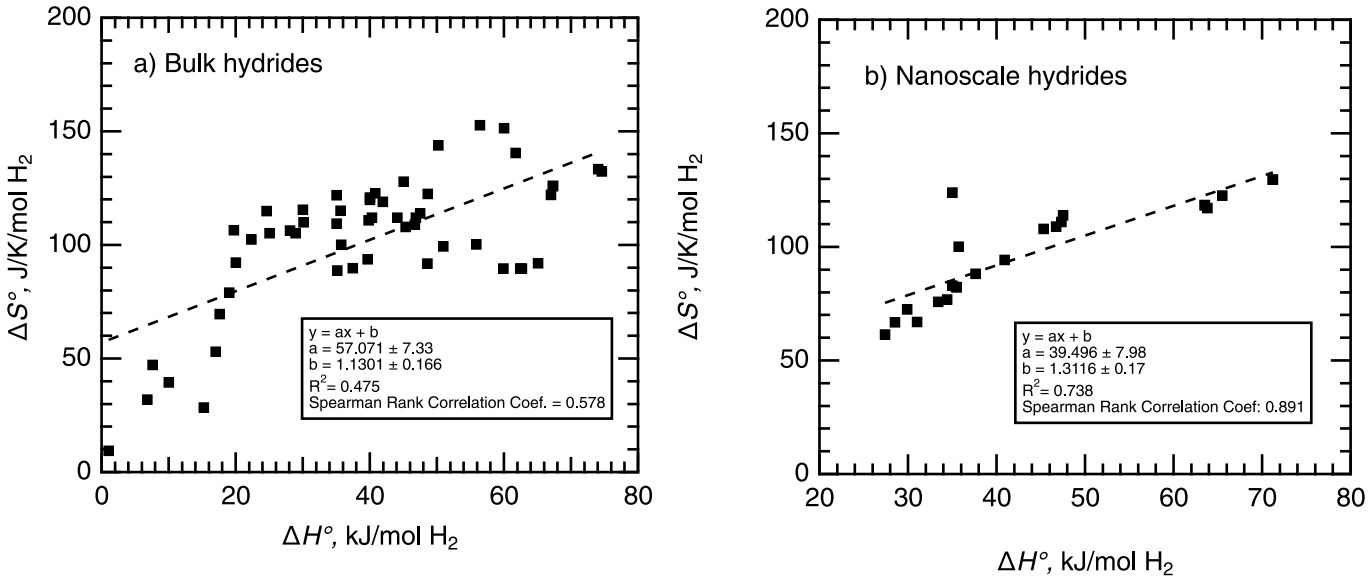

Extended Data Fig. 1 | Linear regression of entropy and enthalpy of dehydrogenation for bulk and nanoscale hydrides. Figure 1 shows linear least-squares fits to the thermodynamic data for (a) bulk and (b) nanoscale hydrides. The bulk data, which are a subset of the full HydPARK database[10], at best show a weak correlation between the entropy $\Delta S°$ and enthalpy $\Delta H°$ of H_2 dehydrogenation, as indicated by the low values of R^2 and the Spearman Rank Correlation Coefficient R. Excluding outlier compositions, as detailed in Ref. [10], improves the fit somewhat, yielding $R^2 = 0.42$ and R=0.68 across the entire ML-ready HydPARK dataset, suggesting a moderate correlation. In contrast, the data for nanoscale hydrides, although admittedly limited, exhibit a fairly strong correlation, with $R^2 = 0.738$ and $R = 0.891$. Within specific hydride classes, stronger $\Delta H°$ and $\Delta S°$ correlations can be found. For example, for nano-PdH $R^2 = 0.954$ and $R = 0.939$ and for bulk AB materials $R^2 = 0.924$ and $R = 0.964$.Source data